Improved cleaning performance of membrane modules using feed spacers modified with cold-plasma treatment and polydopamine and silver-nanoparticle coatings

Huisman, Kees Theo; Abdellah, Mohamed H.; Alvarez Sosa, Damaris S.; Fernandes Simoes, Filipa R.; Blankert, Bastiaan; Vrouwenvelder, Johannes S.; Szekely, Gyorgy

DOI
10.1016/j.desal.2024.117604

Publication date
2024

Document Version
Final published version

Published in
Desalination

Citation (APA)
Huisman, K. T., Abdellah, M. H., Alvarez Sosa, D. S., Fernandes Simoes, F. R., Blankert, B., Vrouwenvelder, J. S., & Szekely, G. (2024). Improved cleaning performance of membrane modules using feed spacers modified with cold-plasma treatment and polydopamine and silver-nanoparticle coatings. *Desalination*, *582*, Article 117604. https://doi.org/10.1016/j.desal.2024.117604

Desalination 582 (2024) 117604

Contents lists available at ScienceDirect

Desalination

journal homepage: www.elsevier.com/locate/desal

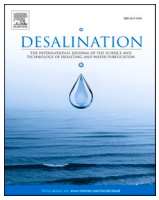

Improved cleaning performance of membrane modules using feed spacers modified with cold-plasma treatment and polydopamine and silver-nanoparticle coatings

Kees Theo Huisman [a,b], Mohamed H. Abdellah [c], Damaris S. Alvarez Sosa [a,b], Filipa R. Fernandes Simoes [a], Bastiaan Blankert [a], Johannes S. Vrouwenvelder [a,b,d], Gyorgy Szekely [c,e,*]

[a] Water Desalination and Reuse Center, Biological and Environmental Science and Engineering Division (BESE), King Abdullah University of Science and Technology (KAUST), Thuwal 23955-6900, Saudi Arabia
[b] Environmental Science and Engineering Program, Biological and Environmental Science & Engineering (BESE) Division, King Abdullah University of Science and Technology (KAUST), Thuwal 23955-6900, Saudi Arabia
[c] Advanced Membranes and Porous Materials Center, Physical Science and Engineering Division (PSE), King Abdullah University of Science and Technology (KAUST), Thuwal 23955-6900, Saudi Arabia
[d] Delft University of Technology, Faculty of Applied Sciences, Department of Biotechnology, Van der Maasweg 9, 2629 HZ Delft, the Netherlands
[e] Chemical Engineering Program, Physical Science and Engineering Division (PSE), King Abdullah University of Science and Technology (KAUST), Thuwal 23955-6900, Saudi Arabia

HIGHLIGHTS

- Cold-plasma treatment enables hydrophilic modification of hydrophobic feed spacers.
- Hydrophilic and biocidal coatings were grafted onto cold-plasma-treated feed spacers.
- Coatings were tested for biofouling control under industrial operating conditions.
- Hydrophilic and biocidal coatings improved the cleaning-in-place effectiveness.
- Improved cleaning effectiveness was maintained over several operational cycles.

GRAPHICAL ABSTRACT

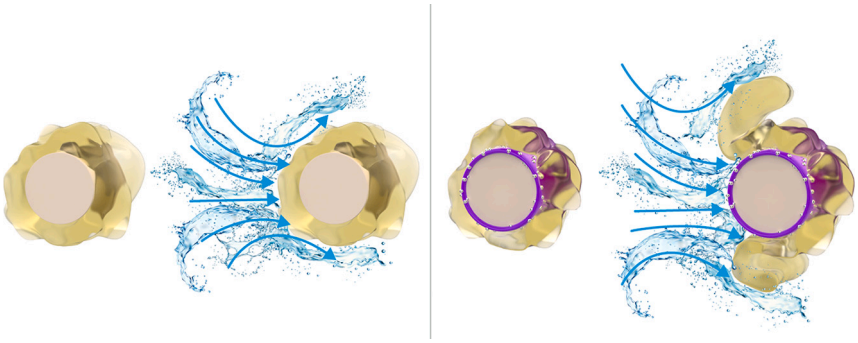

ARTICLE INFO

Keywords:
Biofouling
Polydopamine
Plasma
Reverse osmosis

ABSTRACT

Membrane modules for seawater desalination are becoming increasingly important for obtaining clean water with the rising global water scarcity. The productivity of membrane modules is compromised by biofouling on the membrane and feed spacer. Biofouling development can be mitigated by modification of the spacer or membrane surface. The purpose of the present study is to evaluate the impact of surface-modified feed spacers on

* Corresponding author at: Advanced Membranes and Porous Materials Center, Physical Science and Engineering Division (PSE), King Abdullah University of Science and Technology (KAUST), Thuwal 23955-6900, Saudi Arabia.
E-mail address: gyorgy.szekely@kaust.edu.sa (G. Szekely).
URL: http://www.szekelygroup.com/ (G. Szekely).

https://doi.org/10.1016/j.desal.2024.117604
Received 23 February 2024; Received in revised form 27 March 2024; Accepted 3 April 2024
Available online 4 April 2024

Nanofiltration
Optical coherence tomography

the cleaning performance of spiral-wound membrane filtration systems. After cold-plasma treatment, the feed spacers were modified with various combinations of polydopamine (PDA) and silver nanoparticles (AgNP). To compare the cleaning performance of the modified and unmodified spacers, membrane fouling simulators containing nanofiltration membranes and feed spacers were tested under industrially representative conditions: two full cycles involving biofilm development followed by cleaning-in-place (CIP). The modified spacers significantly improved the CIP efficiency when compared with that of the unmodified feed spacer. The highest CIP efficiency was obtained for the PDA–AgNP-coated spacers, which removed >90 % of the biomass. The PDA layers remained undetached during the CIP process, and the amounts of AgNP decreased without affecting the CIP effectiveness during consecutive operational cycles. The results demonstrate that CIP should be included in biofouling tests to evaluate the full potential of surface modifications and suggest that hydrophilic and biocidal spacer surface coatings can significantly improve the CIP effectiveness, thereby considerably reducing the CIP frequency and operational costs.

1. Introduction

While freshwater is increasingly demanded due to population growth and economic development, its availability is decreasing due to desertification and pollution. Therefore, seawater desalination and closing urban water cycles (through e.g., wastewater reuse [1]) are becoming increasingly important [2] for achieving the United Nations' Sustainable Development Goals such as the one on access to clean water for all. Spiral-wound membrane technologies such as reverse osmosis and nanofiltration are globally applied to produce high-quality water from seawater, brine, and wastewater. The spiral-wound modules include a feed spacer sandwiched between two membrane sheets to provide structural stability for the feed channel. The feed spacer also reduces concentration polarization by improving mass transfer toward the bulk; on the downside, it increases the feed pressure due to drag forces [3]. Moreover, the spacer can play an important role in fouling development in the feed channel, especially biofouling, which is commonly present as a layer around the spacer filaments [4]. Biofouling results from the excessive development of bacterial biofilms, which causes an intolerable decrease in operational performance and an increase in operating costs [5,6].

Continuous efforts have been dedicated to mitigating biofouling over the last decade, including preventative measurements such as feed spacer design including, arch-type [7], column-type [8], and honeycomb [9] geometries, and surface modification and corrective measurements such as chemical and mechanical cleaning [10]. Modifying spacer surfaces with anti-adhesive or anti-bacterial coatings is considered a promising strategy for biofouling mitigation [11–14]. In short-term static adhesion experiments, researchers observed that hydrophilic and biofilm-disrupting compounds strongly reduce the adhesion of bacteria and biopolymers to coated surfaces [15–17]. However, in long-term experiments in continuous-flow environments where bacteria, biopolymers, and nutrients are constantly supplied, biofouling is more likely than in short-term static adhesion tests. Moreover, impacts of residual chemicals from the coating procedure are less likely in continuous-flow tests than in static adhesion tests, as they are flushed out rather than retained in the static volume.

Long-term studies in membrane fouling simulators have yielded mixed results, some studies observed a decrease in cell attachment and permeate flux decline for AgNP spacer coatings [18,19], whereas others found no decrease in feed channel pressure drop and biofouling development for PDA and copper spacer surface modifications [17,20]. Although several studies have evaluated the impact of hydrophilic and biocidal coatings on biofilm development, the impact on cleaning-in-place (CIP) performance is unknown.

CIP is a key strategy for mitigating biofouling in industrial membrane filtration. CIP is recommended when the trans-membrane pressure increases by 15 %, the salt passage increases by 10 %, or the feed channel pressure drop increases by 15 % [21]. Frequent CIP can reduce the membrane integrity and lifetime, increase operational costs, and cause environmental damage [22,23]. These problems can be reduced by optimizing the CIP frequency of spiral-wound membrane filtration systems. Hydrophilic and anti-bacterial coatings may weaken the adhesive strength of bacteria and biopolymers [17], resulting in biofouling that is easier to clean and enables a larger performance recovery resulting in a lower cleaning frequency.

The goal of the current study was to evaluate the impact of hydrophilic and biocidal feed spacer coatings on the CIP performance. Polymerized dopamine (PDA) was selected as coating agent as it is commonly applied owing to its strong adherence to wetted surfaces, hydrophilicity, easy application, and ability to sequester nanoparticles [24]. Silver nanoparticles (AgNP), which were found to have the most antimicrobial activity compared with other metals [25], were selected as biocidal compounds as it has shown active biofilm-disrupting ability and good adhesion to PDA [15–17,20,26]. The (i) biofilm development, (ii) structural properties, and (iii) CIP performance of modified spacers were tested in long-term fouling experiments under industrially relevant operating conditions (crossflow velocity, permeate flux, and periodic CIP). Insight into the behavior of PDA- and AgNP-modified feed spacers during CIP events will be helpful in engineering anti-fouling spacer coatings that are effective in "real-life" systems.

2. Materials and methods

Commercial spacers were treated with cold plasma and coated with different combinations of PDA and AgNP (see Fig. 1a). The operational and CIP performances were evaluated by monitoring the feed-channel pressure drop and imaging with optical coherence tomography (OCT) (Fig. 1b). The physical and chemical properties of the coated spacers were characterized before the biofouling experiment using atomic force microscopy (AFM), scanning electron microscopy (SEM) with energy dispersive X-ray spectroscopy (EDX), contact-angle measurements, and Fourier transform infrared spectroscopy (FTIR). The amount of AgNP on the feed spacers was evaluated before and after the experiment using inductively coupled plasma mass spectrometry (ICP–MS).

2.1. Materials

Dopamine hydrochloride (98 %), sodium acetate (99.5 %), sodium nitrate (99 %), sodium phosphate (99 %), sodium hydroxide (98 %), silver nitrate (99 %), and sodium periodate (99.8 %) were obtained from Sigma Aldrich. Nitric acid (69 %) was purchased from VWR chemicals, trace-metal grade hydrochloric acid (37 %) was obtained from Fisher Chemicals, and a single stock solution of silver (100 μg mL^{-1}) was obtained from Inorganic Ventures. All solutions were prepared and diluted using deionized water (resistivity = 18 MΩ) using a water purification system (Milli-Q, Merck, USA). Nanofiltration membrane sheets (FILMTEC NF90) were obtained from Dupont (USA) and commercial polypropylene (PP) feed spacers were obtained from DelStar Technologies (USA). All chemicals were used as received without further purification.

2.2. Surface modification

The feed spacer was cut into rectangular (40 × 200) mm^2 coupons to

fit the experimental setup. The spacer surface was activated by treating each coupon once with atmospheric cold plasma for 5 min at 300 W. The coupons were then immersed in 2 g L^{-1} dopamine hydrochloride solution at 25 °C and placed on a shaker for 24 h. After adding sodium periodate to a concentration of 5 mM, the mixture was left on the shaker for another 24 h to form a single-layer coating [27,28]. This procedure was repeated to achieve a double-layer coating as a remedy for any defects that may be present in the single-layer coating. Next, the PDA-coated spacers were immersed in 100 mM silver nitrate solution and placed on the shaker for 24 h for AgNP immobilization [29]. For each of the four spacers prepared under specific conditions (see Table 1 and Fig. 1 for details), a flat PP film was treated under the same conditions for water contact angle measurements and AFM, which cannot be performed on the spacers themselves.

The cold plasma treatment of PP spacers activates the surfaces through the generation of active functional groups such as –OH and –O. This activated surface enhances the binding of dopamine monomers [30]. Upon the introduction of sodium iodate as an oxidizing agent, dopamine undergoes self-polymerization. Initially, the two hydroxyl groups undergo deprotonation, leading to the formation of dopamine-quinone. Subsequent cyclization, oxidation, and rearrangement transform it into 5,6-dihydroxyindole. This compound further undergoes deprotonation and polymerization via Michael addition reactions, resulting in the formation of a cross-linked polydopamine polymer [31]. The active phenolic groups (–OH) present in the polydopamine reduce the silver ions present in the solution upon the addition of silver nitrate and convert them to atomic silver nanoparticles which bind to the polydopamine layer [32].

Table 1
Treatment procedures and the obtained spacer materials.

Tag	Treatment procedure	Material
S^{Ctrl}	None	Benchmark spacer
S^{PDA}	Plasma (300 W, 5 min) Dopamine hydrochloride (2 g L^{-1}, 24 h) Sodium periodate (5 mM, 24 h)	Spacer with a single layer of PDA
S^{PDA-Ag}	Plasma (300 W, 5 min) Dopamine hydrochloride (2 g L^{-1}, 24 h) Sodium periodate (5 mmol, 24 h) Silver nitrate (100 mM, 24 h)	Spacer with a single layer of PDA with immobilized AgNP
S^{2PDA}	Plasma (300 W, 5 min) Dopamine hydrochloride (2 g L^{-1}, 24 h) Sodium periodate (5 mM, 24 h) Dopamine hydrochloride (2 g L^{-1}, 24 h) Sodium periodate (5 mM, 24 h)	Spacer with two layers of PDA
$S^{2PDA-Ag}$	Plasma (300 W, 5 min) Dopamine hydrochloride (2 g L^{-1}, 24 h) Sodium periodate (5 mM, 24 h) Silver nitrate (100 mM, 24 h) Dopamine hydrochloride (2 g L^{-1}, 24 h) Sodium periodate (5 mM, 24 h)	Spacer with two layers of PDA separated by AgNP
S^{Ag}	Plasma (300 W, 5 min) Silver nitrate (100 mM, 24 h)	Spacer with AgNP

2.3. Spacer characterization

The spacer morphologies were determined from the surface and cross-sectional SEM images obtained with a Magellan instrument (acceleration voltage = 5 kV, current = 0.1 pA). Before imaging, the samples were snapped in liquid nitrogen, fixed on the stub using copper tape, and rendered electrically conductive by coating with a 4-nm-thick platinum layer using a Q150TES instrument (Quorum Technologies, UK) under an Ar atmosphere. The EDX mappings of C, N, O, and Ag on the

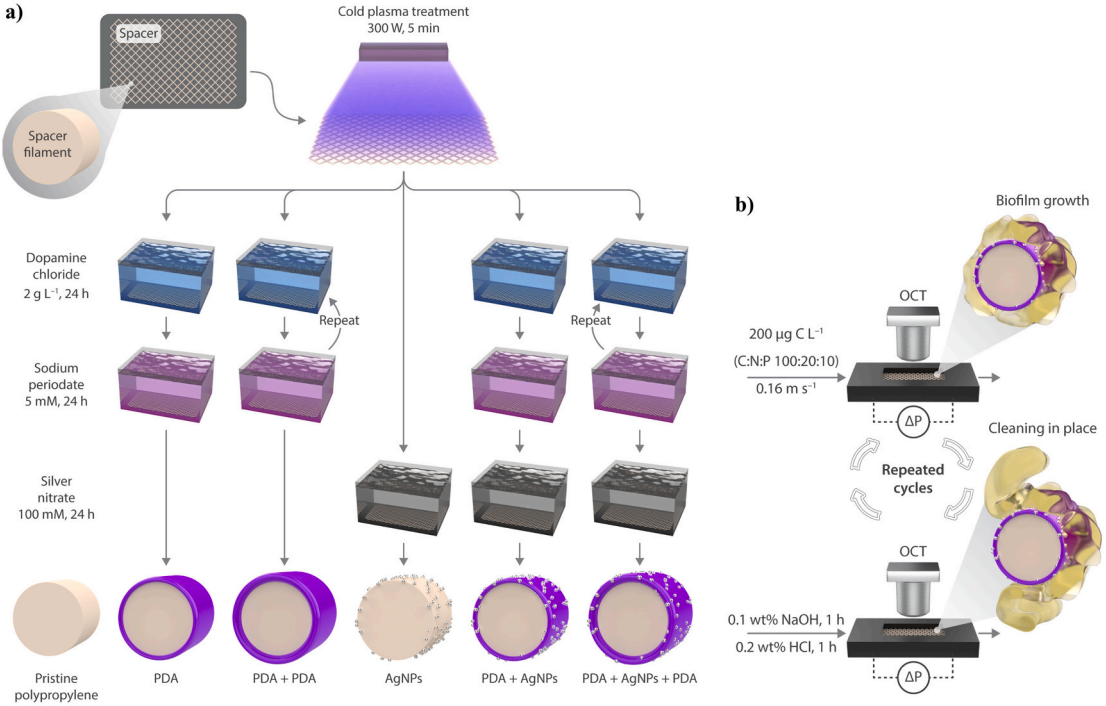

Fig. 1. Experimental design and procedure. a) Polypropylene spacers were treated with cold plasma and coated with polydopamine (PDA) and silver nanoparticles (AgNP). b) Spacers were tested for their impact on biofilm growth and cleaning-in-place (CIP) under industrial operating conditions. Biofouling was monitored with pressure drop measurements (ΔP) in the feed channel and by imaging with optical coherence tomography (OCT).

samples were obtained using a Magellan instrument with an acceleration voltage and current of 10 kV and 0.8 nA, respectively. The FTIR attenuated total reflection of the spacers was analyzed through 32 scans of an Alpha-P instrument (Bruker Instruments, USA) in the 600–4000 cm^{-1} range. The water-contact angles of the PP films were measured by the sessile drop method using an EasyDrop instrument (Kruss Scientific, DE) and the Young–Laplace fitting model. Before analysis, the samples were fixed on a clean glass plate using double-sided tape, and 4-μL water droplets were gently placed at different locations on each sample. The surface roughness values of the PP films were analyzed using AFM images (BioAFM Multimode 8 instrument, Bruker, USA) obtained in the standard tapping mode in the air at 25 °C on an area of (20 × 20) μm^2 with a scanning rate of 1 Hz. The average mean squared roughness (R_{sq}) was analyzed using Gwyddion software. The Ag on the spacers was quantified using ICP–MS (Agilent 8800, Agilent Technologies, USA). Before measurement, the samples were acid-digested using an Ultrawave Microwave Digestion chamber (Milestone Srl, IT). The digestion was performed in a mixture of concentrated nitric acid and hydrochloric acid (ratio 4:1) for 40 min under high pressure (40 bar) at 250 °C. The vessels were kept closed at room temperature for 1 h. The samples were then transferred to 50-mL vials and diluted with deionized water.

2.4. Biofouling test

2.4.1. Setup

The biofouling test was set up as described in [33]. Briefly, tests were performed in membrane fouling simulators with an active membrane area of 0.08 m^2 and a channel height determined by the feed spacer (nominal thickness = 34 mil or 863 μm). The six different spacers were tested simultaneously in membrane fouling simulators operated in parallel. The hydrodynamic conditions, crossflow velocity, permeate flux, and development of pressure drop of these simulators represented those in spiral-wound nanofiltration modules [34–36]. The feed spacers were angled approximately 45° from the flow direction of the feed, as is common in spiral wound membrane elements [11]. The simulators were installed with an optical window for OCT imaging of biofouling in the feed channel. To measure the pressure drop in the feed channel, the inlet and outlet of the feed channel were connected to a differential pressure transmitter.

Local tap water produced by seawater reverse osmosis was filtered through a granular activated carbon filter and a filtration cartridge to remove residual chlorine. The feed water contained typical ions such as calcium and sodium ions and was enriched with nutrients to accelerate the biofouling process. The feed-flow rate and nutrient-dosing setpoints were maintained using gear pumps coupled to mass-flow transmitters and controllers. To sustain the permeate flux, the concentrate pressure was regulated through a pressure controller coupled to a mass-flow meter.

2.4.2. Experimental procedure

Membrane sheets were conditioned with filtered tap water at a superficial velocity of v_{sp} = 0.16 m s^{-1} and a permeate flux of J_{sp} = 20 L m^{-2} h^{-1} for seven days before the experiment. The experiment consisted of two consecutive operational cycles. Each operational cycle involved a biofilm development stage followed by CIP.

During the biofilm development stage, filtered tap water was fed to the membrane fouling simulators at v_{sp} = 0.16 m s^{-1} and J_{sp} was maintained at 20 L m^{-2} h^{-1}, which are representative operating conditions for industrial practice [36,37]. To accelerate the biofilm development, the tap water was continuously enriched with sodium acetate, sodium nitrate, and sodium phosphate. The feed concentration was 200 μg C L^{-1} with a C:N:P mass ratio of 100:20:10. The nutrients were dosed from a 10-L stock solution using deionized water. To avoid bacterial growth in the solution, the pH was raised to 11 by adding sodium hydroxide. The high pH of the stock solution did not change the pH of the feed solution because the flow rate of the dosed nutrients was much lower than the feed-flow rate.

The CIP was initiated when the pressure drop increased by 100 % relative to the pressure drop of the virgin channel. In accordance with industrial practice, during the CIP permeate production was paused, and feed water was displaced with 0.1 wt% NaOH (pH = 12) followed by 0.2 wt% HCl (pH = 1) recirculated at v_{sp} = 0.16 m s^{-1} for 1 h each [21]. The NaOH solutions were maintained at 35 °C, the typical temperature in the industry [21].

2.4.3. Performance monitoring

The performance was monitored with two parameters: the biofouling index and CIP effectiveness. Detailed information on the biofouling index may be found in previous work [33]. In brief, the biofouling index (BFI) was defined as the inverse of the time (t^*) required for a pressure drop increase of 100 % relative to the pressure drop in the virgin channel:

$$BFI = \frac{1}{t^*} \tag{1}$$

The relative pressure drop (RPD) is a proxy of biofouling volume in the spacer-filled feed channel [33]. It is determined from the pressure drop PD_t and the initial pressure drop PD_0 as follows:

$$RPD = \frac{DP_t - DP_0}{DP_0} \bullet 100\% \tag{2}$$

In industrial practice, CIP is recommended when the RPD over a vessel reaches 15 % [21]. A vessel typically consists of seven or eight membrane modules with most of the fouling (and consequent pressure drop) occurring in the lead module [35,38,39]. As a 15 % RPD in the vessel may correspond to approximately 100 % RPD in the lead module, a 100 % RPD in the membrane fouling simulator likely represents the biofouling condition in the lead module when CIP is recommended. The biofouling index can be interpreted as the biofouling rate or CIP frequency. The measured CIP frequency in the accelerated biofouling experiment qualitatively indicates the expected CIP frequency of industrial practice. The CIP effectiveness (indicating the volume of remaining biofilm) was evaluated as the RPD after CIP.

2.4.4. Optical coherence tomography

The amount and location of biofouling were monitored using an OCT system (GAN610C1, Thorlabs GmbH, DE) with a central light-source wavelength of 930 nm. The system was configured for imaging with a refractive index of 1.33 and an A-scan rate of 36 kHz. To improve the image quality, the noise floor was flattened with an A-scan averaging of 20 and a B-scan averaging of 10. OCT images were obtained before and after CIP at the same location selected a priori. The volumetric images had a resolution of 499 × 499 × 558 voxels and a field of view of 5.0 mm × 5.0 mm × 1.2 mm. From the images, the same location with reference to each spacer cell was selected using a customized Matlab® (MathWorks, USA) script for systematic comparison [40,41].

3. Results

3.1. Characterization of spacers and coatings

Dopamine is a bioderived material belonging to the catecholamine family. It consists of catechol with a primary-amine-group side chain (Fig. 2a). Among the catecholamines, dopamine exhibits the highest oxidation potential. Dopamine can be oxidized to dopamine quinone (dihydroxy indole), which self-polymerizes into an insoluble PDA network (Fig. 2a). Successful coating of PDA on the spacers was confirmed through FTIR analysis (Fig. 2b). The FTIR spectrum of pristine PP shows strong peaks at 1376 and 1450 cm^{-1} corresponding to the symmetrical bending of $–CH_3$. The peak at 2867 cm^{-1} corresponds to $–CH_3$ stretching while the peaks at 2917 and 2951 cm^{-1} correspond to asymmetric $–CH_3$ stretching. The spectrum of S^{Ag} was identical to that of

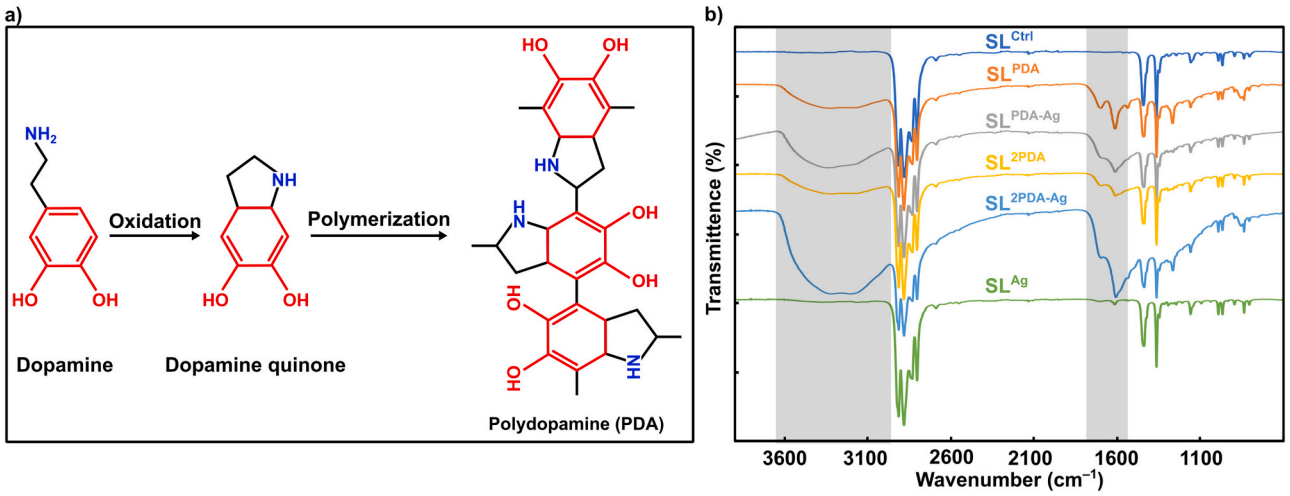

Fig. 2. a) Polymerization reaction of dopamine to polydopamine (PDA) and b) FTIR analysis of the modified feed spacers.

the control, indicating that PP acquired no new functional groups after treatment with plasma and silver nitrate. In contrast, the spectra of the dopamine-treated S^{PDA}, $S^{PDA\text{-}Ag}$, S^{2PDA}, and $S^{2PDA\text{-}Ag}$ samples showed a new broad peak in the 3000–3600 cm^{-1} range, which corresponds to the –OH group in the catechol unit of PDA. Meanwhile, the sharp peak at 1625 cm^{-1} corresponds to N–H vibrations in the PDA structure. The FTIR analysis confirmed the successful polymerization of dopamine and the coating of spacers with a PDA film.

The catechol units in the PDA unit (red parts in Fig. 2a) immobilize metal nanoparticles by reducing their ions in solution. Here, AgNP was immobilized on the PDA film after soaking the coated spacers (S^{PDA} and S^{2PDA}) in a 100-mM aqueous solution of silver nitrate. The presence of AgNP on the spacers was examined using EDX (Fig. S1 of the Supporting Information). The spectra of all samples showed a strong peak of C, the main component of the spacer, and an Ir/Zr peak corresponding to the conductive film-like coating. The spectra of the PDA-coated samples (S^{PDA}, $S^{PDA\text{-}Ag}$, S^{2PDA}, and $S^{2PDA\text{-}Ag}$) showed additional O and N peaks contributed by the PDA structure. The Ag peaks in the spectra of $S^{PDA\text{-}Ag}$ and $S^{2PDA\text{-}Ag}$ confirm the successful immobilization of AgNP on the PDA film. The weak Ag peak in the $S^{2PDA\text{-}Ag}$ spectrum can be explained by partial leaching of the AgNP after coating with the second PDA film. The Ag peak was negligible in the S^{Ag} spectrum, likely because S^{Ag} lacks a strong reducing agent. In contrast, the catechol units in $S^{PDA\text{-}Ag}$ and $S^{2PDA\text{-}Ag}$ are relatively strong reducing agents for the formation of Ag NPs from silver ions.

Panels a–f of Fig. 3 show cross-sectional SEM images of the samples. The SEM images of S^{PDA}, $S^{PDA\text{-}Ag}$, S^{2PDA}, and $S^{2PDA\text{-}Ag}$ showed a dense PP structure coated with a thin film (indicated by black arrows). The thicknesses of the coating films were roughly measured using ImageJ software, obtaining 247 ± 15 nm, 263 ± 36 nm, 348 ± 22 nm, and 277 ± 13 nm for S^{PDA}, $S^{PDA\text{-}Ag}$, S^{2PDA}, and $S^{2PDA\text{-}Ag}$ respectively. The spacer coating thicknesses were negligible compared to the spacer thickness of 863 μm. Hence, the impact of the spacer coatings on the feed channel pressure drop was negligible. The surface images of most samples

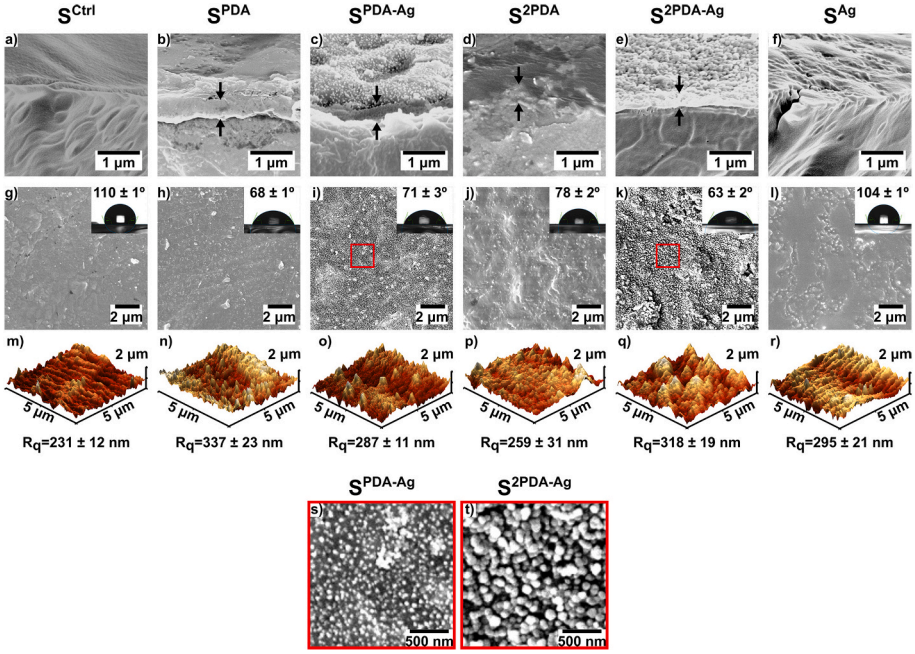

Fig. 3. Cross-sectional (a–f) and surface (g–l, s, and t) SEM images and AFM images of the PP films (m–r). The insets in g–l show the water-contact angles of the PP films. Higher magnification surface images of s) $S^{PDA\text{-}Ag}$ and t) $S^{2PDA\text{-}Ag}$ within the area surrounded by the red square in i) and k), respectively. (For interpretation of the references to color in this figure legend, the reader is referred to the web version of this article.)

(Fig. 3g–l) showed a uniform morphology; the exceptions were S^{PDA-Ag} and $S^{2PDA-Ag}$, which presented spheroidal particles (Fig. 3s and t) representing the AgNP. The spheroidal particles were larger on $S^{2PDA-Ag}$ than on S^{PDA-Ag}, with average diameters of 119 ± 8 nm and 57 ± 5 nm, respectively. The increased particle size on $S^{2PDA-Ag}$ was attributed to the extra PDA layer covering the AgNP (see Table 1), because the PDA film S^{PDA} introduced more roughness than the silver-containing S^{PDA-Ag}. The AFM images (Fig. 3m–r) show the topologies of the materials. The roughness was increased after applying the coatings to the smooth pristine PP spacer. As PP is a hydrophobic polymer with no hydrophilic groups, its water-contact angle is 110° ± 1°. The PDA and AgNP coatings improved the wettability of spacers S^{PDA}, S^{PDA-Ag}, S^{2PDA}, and $S^{2PDA-Ag}$, reducing the water-contact angles to 63°–68°. The decreased contact angles were attributed to the hydroxyl (–OH) and amino (–NH) groups in the PDA structure (see Fig. 2a), which facilitated bonding between the spacers and water molecules, thereby improving the hydrophilicity of the spacers. The water contact angle of S^{Ag} was negligibly increased because no strong hydrophilic groups existed on the surface of this spacer. The contact angle of the surface is mainly affected by the surface roughness and chemistry [42]. According to the Wenzel model, when the surface is hydrophilic, the apparent contact angle decreases with the increasing surface roughness. On the other hand, the contact angle increases with increasing the roughness of the hydrophobic surface. The presence of hydrophilic or hydrophobic groups on the surface of the material may have opposing or supporting effects to that of roughness. It was found that the presence of acid functional group on the surface of silicon-based substrate decreased the water contact angle although the surface roughness was increased [43].

3.2. Biofouling test

This test investigated the impacts of the PDA and AgNP coatings (Table 1) on biofilm formation and CIP. The performance of the coatings was evaluated in long-term biofouling experiments using membrane fouling simulators. The biofouling experiment entailed two consecutive operational cycles of biofilm development followed by CIP. The CIP was performed when the pressure drop due to biofouling increased by 100 % relative to that in the virgin feed channel.

3.2.1. Biofouling development

Fig. 4a shows the biofouling indices during the first and second operational cycles. The indices of the modified and unmodified spacers only marginally differed during the biofouling of the virgin channels in the first cycle. In industrial practice, biofilm regrowth after CIP necessitates many consecutive cycles of this process. The CIP criterion is reached earlier if the CIP is less effective, and more biofouling remains in the channel. For this reason, the second cycle is more relevant to industrial practice. The biofouling index of all spacers was significantly higher after the second cycle than after the first cycle. Moreover, the indices substantially differed between the unmodified control and the coated spacers. $S^{2PDA-Ag}$ achieved the lowest biofouling rate, approximately 33 % lower than that of the control. The PDA coating significantly lowered the biofouling rates of S^{PDA}, S^{PDA-Ag}, S^{2PDA}, and $S^{2PDA-Ag}$ from that of the control. In contrast, the biofouling rate of the AgNP-modified spacer (S^{Ag}) was not significantly reduced from that of the control.

Fig. 4b-g shows the OCT images of biofouling in the feed channels during the first and second CIP at an RPD of approximately 100 %. Most of the biofouling was located around the spacers. No substantial differences were observed between the amounts of biofouling on the unmodified and modified spacers, suggesting that the coatings did not prevent biofouling on the spacer surface.

3.2.2. CIP effectiveness

When the feed channel pressure drop increased by approximately 100 % relative to the pressure drop in the virgin channel, NaOH was recirculated for 1 h followed by HCl for 1 h. Fig. 5a shows the RPDs after CIP during the first and second operational cycles. The RPD after CIP represents the volume of biofouling remaining on the membrane and spacer. After the first operational cycle, substantially less biofouling remained on the modified spacers than on the unmodified control. Approximately 10 % of the biofouling remained after the CIP of the spacers modified with both PDA (S^{PDA} and S^{2PDA}) and PDA with AgNP (S^{PDA-Ag} and $S^{2PDA-Ag}$). The AgNP coating (S^{Ag}) also outperformed the control (S^{Ctrl}) (remaining biofouling ~30 % versus ~45 %). The effectiveness of CIP at the ends of the first and second operational cycles was similar on the spacers modified with PDA and AgNP (S^{PDA-Ag} and $S^{2PDA-Ag}$) but the amounts of remaining biofouling on the other modified spacers and the unmodified control after CIP were higher after the second operational cycle than after the first. Nevertheless, the amount of biofouling after CIP was substantially lower on the modified spacers than on the control, suggesting that coated spacers can significantly improve the CIP effectiveness.

Fig. 5c–h shows the accumulation of biofouling in the spacer cells after the first CIP, computed from OCT images using a method based on Fortunato et al. [44]. The results confirm that less biofouling remained on the modified feed spacers than on the unmodified spacer (Fig. 5a). To evaluate the impact of the amount of remaining biofouling after CIP on the biofouling index, the remaining biofouling after the first operational cycle was plotted against the biofouling index during the second cycle

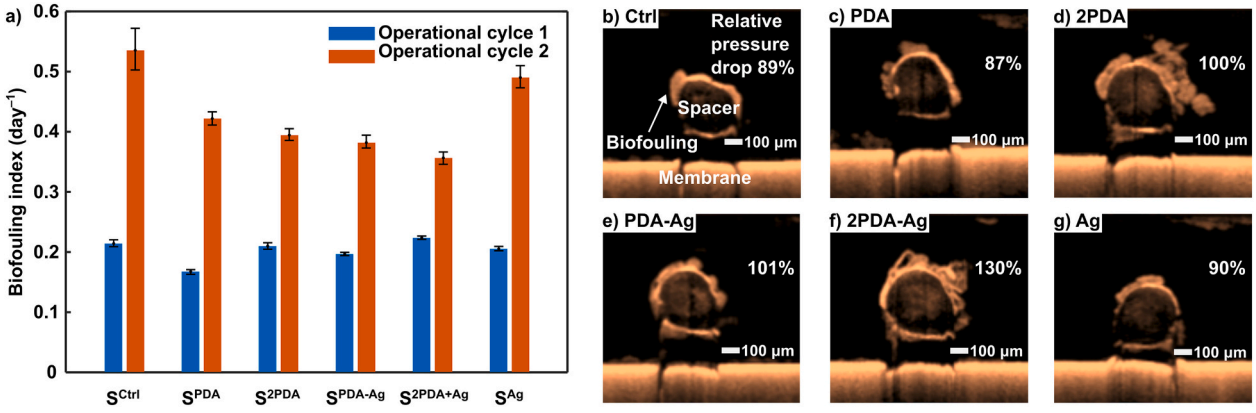

Fig. 4. Biofouling development on modified spacers and the unmodified control during the first and second operational cycles. A) The biofouling indices (see Section 2.4.3) during the first cycle were similar (0.20 ± 0.02). During the second cycle, the PDA-modified spacers (S^{PDA}, S^{PDA-Ag}, S^{2PDA}, and $S^{2PDA-Ag}$) presented substantially lower biofouling rates than the control. The error bars show the propagation of the measurement error of the pressure drop transmitter (1 mbar). (b–g) Cross-sections from 3D OCT images showing biofouling on the control and modified spacers. The images were selected for illustrative purposes at different RPD values.

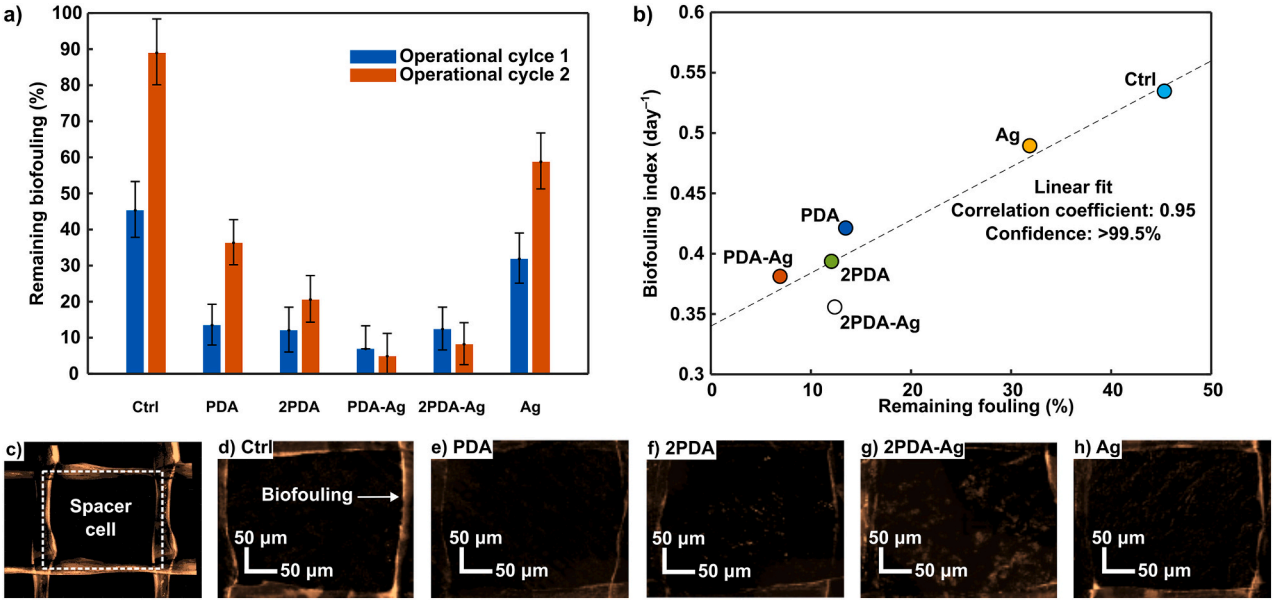

Fig. 5. CIP effectiveness of the modified spacers and the unmodified control during the first and second operational cycles. CIP was performed when the initial pressure drop increased by 100 %. A) RPD after CIP, representing the amount of biofouling remaining after CIP. The spacer coatings improved the biofouling removal during CIP compared to the control. The error bars show the propagation of the measurement error of the pressure drop transmitter (1 mbar). B) Remaining biofouling after the first operational cycle versus biofouling index during the second cycle. The modified spacers significantly reduced the biofouling rate by improving the CIP performance. (c–h) Accumulation of biofouling in the spacer cells, evidenced by OCT images after the first CIP. The lower color intensity around the modified spacers than around the pristine spacer indicates less accumulation of biofouling on the modified spacers.

(Fig. 5b). The amount of biofouling remaining was strongly correlated with the interval until CIP was required. This finding shows that the modified spacers can reduce the CIP frequency by improving the CIP performance.

3.2.3. *Coating stability*

The leaching of AgNP from the coated spacers was evaluated through quantification of the amount of AgNP on the spacer through ICP–MS (Table 2). Samples were taken before the start and at the end of the experiment (after 8 days). After acid digestion, all samples were free of visible residues, indicating a highly efficient digestion process [45]. The ICP–MS analysis confirmed that the PDA layers improved the adhesion of AgNP during the coating procedure. The AgNP concentration was higher on $S^{PDA–Ag}$ than on $S^{2PDA–Ag}$, possibly because some AgNP might have detached from the surface during the second dip-coating to achieve the double PDA layer. During the experiment, 83 %, 92 %, and 97 % of the initial AgNP deposited on the spacer was released to the bulk for respectively S^{Ag}, $S^{PDA–Ag}$, and $S^{2PDA–Ag}$. Despite the release of AgNP, the CIP performance of $S^{PDA–Ag}$, and $S^{2PDA–Ag}$ was not compromised during the second operational cycle (Fig. 5a).

The presence of PDA on the spacer was not quantified. However, the characteristic brown color of PDA could be used as a qualitative indicator of the presence of PDA. As shown in Fig. S2 of the Supporting Information, the PDA-modified spacers exhibited the brown color before the start of the first CIP. After the first CIP, the color of the spacers showed no apparent change, suggesting that the PDA layer remained on the spacer during CIP.

Table 2
Amount of AgNP on the spacer surfaces before and after the experiment quantified with ICP-MS. The amount is presented in percentage AgNP weight per spacer weight. The weight loss during the experiment is expressed as percentage of the initial amount.

Spacer tag	Initial amount of AgNP (% ***w***/w)	Final amount of AgNP (% w/w)	Weight loss (%)
S^{Ctrl}	0.000	0.000	0
S^{Ag}	0.007	0.001	83
$S^{PDA–Ag}$	0.169	0.013	92
$S^{2PDA–Ag}$	0.094	0.003	97

4. Discussion

This study aimed to evaluate the biofouling development and CIP effectiveness of spacer coatings during long-term biofouling tests in membrane fouling simulators with permeation and intermittent chemical CIP. Commercial PP feed spacers were coated with single and double layers of PDA, AgNP, AgNP deposited on single-layered PDA, and AgNP sandwiched between two layers of PDA (Table 1). Biofilm development was monitored with pressure-drop measurements and OCT imaging of the tested spacer coatings. The CIP performance was significantly better for spacers coated with PDA or PDA–AgNP than for the uncoated control. Consequently, the CIP frequency for biofilm regrowth was significantly reduced on the PDA- and PDA and AgNP-coated spacers.

4.1. *CIP performance should be included in biofouling tests to evaluate the full potential of surface modifications*

Surface modification is considered a promising strategy for biofouling mitigation on feed spacers [11–13]. In short-term static adhesion experiments, PDA and biofilm-disrupting compounds strongly reduced the adhesion of bacteria and biopolymers to the coated surface [15–17]. Similarly, some long-term tests reported a decrease in cell attachment and permeate flux decline for AgNP spacer coatings [18,19]. However, in one of these studies, the results may have been affected by variations in the seawater feed as the tests were performed in series [18]. Since, seawater composition can vary strongly in time [46], in the current study spacer coatings were tested in parallel. In another study, the AgNP-modified spacer and control spacer showed a similar flux decline during the first 3 days of a biofouling experiment until the normalized permeate flux was decreased by about 50 % [19]. After 3 days, well beyond the cleaning threshold of 15 % normalized flux decline [21], the flux stabilized in the system with a modified spacer. Other long-term experiments in membrane fouling simulators with biocidal and PDA

coatings did not observe a reduction of adhesion or delay in biofouling [17,20]. In continuous-flow environments, hydrodynamic conditions, shear, and turbulence reportedly play a key role in bacterial adhesion and biofilm formation, whereas physicochemical properties, which are also present in static adhesion tests, are less important [20,47–49]. Moreover, continuous-flow experiments are less likely to be affected by residual chemicals from the coating procedure than static experiments, as the chemicals are flushed out rather than retained in the static volume.

Although these long-term experiments in membrane fouling simulators mimic biofouling in full-scale modules, they did not include CIP, which is an important aspect of industrial operation of membrane modules [21]. Hydrophilic and biocidal surface modifications may enhance CIP, resulting in a greater performance recovery, and a lower cleaning frequency.

4.2. Hydrophilic and biocidal spacer coatings enhanced CIP effectiveness

The current study evaluated the impact of CIP of periodic cleaning under conditions representative of industrial practice. The spacers coated with PDA and/or AgNP maintained their adhesive properties and exhibited the same biofouling propensity as the unmodified spacer; that is, they did not delay biofilm formation on the spacer surface. Moreover, it was shown that the spacers coated with PDA and/or AgNP strongly improved the CIP effectiveness. Suggesting that the merits of a spacer coating can lie in improving CIP rather than delaying biofouling. Hence, the development of novel feed spacer and membrane modifications should consist of full operational cycles including periodic cleaning for a full understanding of the anti-biofouling potential of spacer and membrane surface modifications.

The mechanism of chemical cleaning of biofouling consists of (i) mass transfer of cleaning agents from the bulk into the fouling layer and (ii) reaction of cleaning agents with the fouling layer [50]. In industrial practice, a typical cleaning consists of a two-step cleaning with NaOH (pH 12) and HCl (pH 1). Alkaline treatment hydrolyses and solubilizes organic fouling and biofouling whereas acidic treatment dissolves scaling [51]. The influence of local physicochemical conditions such as pH on biofouling is not well known [52]. An important factor may be the extracellular polymeric substances (EPS) matrix, which is thought to be a determinant of biofilm structural and mechanical stability [53]. It is anticipated that a better understanding of the EPS matrix will enable more targeted CIP [53]. The hydrophilic nature of PDA and the antibacterial properties of AgNP can alter the EPS matrix, weakening the cohesive and adhesive forces and facilitating the removability of the biofouling layer [49,54]. Indeed, PDA-based membrane coatings are known to enhance the reversibility of biofouling. In short-term biofouling studies, membranes coated with combined PDA and biocidal compounds showed much higher reversibility than uncoated controls [55–57]. In the current study, the biofouling reversibility was higher for all modified spacers than the unmodified spacer, suggesting that the biofilm cohesion and adhesion were weakened by biotoxicity in the AgNP-coated spacer, hydrophilicity in the PDA-coated spacer, or a combination of both factors in the spacer coated with both PDA with AgNP. It is hypothesized that reduced cohesion and adhesion enable better mass transfer and effectivity of cleaning agents within the biofouling layer. The dual PDA coating with AgNP maximally improved the CIP effectivity and preserved the CIP effectiveness during the second CIP cycle, in contrast to the control and other coatings which showed deterioration of CIP effectiveness in the second cycle. Deterioration of CIP effectiveness is a well-known problem in membrane filtration systems, leading to irreversibly fouled membranes and spacers [58–60]. Our results showed that a small amount of AgNP sequestered by PDA has the potential to mitigate irreversible biofouling, facilitate the CIP, and lower the CIP frequency.

4.3. Follow-up

During the industrial operation of reverse osmosis and nanofiltration modules, drinking water production is alternated with CIP to remove fouling. Feed water sources are usually at neutral pH, whereas CIP usually involves strongly acidic and alkaline CIP agents. The behavior of PDA coatings under strongly acidic and alkaline conditions has rarely been reported. Wibisono et al. [61] observed substantial leaching of various polymer coatings during 30 days of incubation in acidic, neutral, and basic conditions. Yang et al. [62] found that after 1 h of washing with low pH and high pH agents, >50 % and 70 % of the PDA detached from PDA-coated gold surfaces, respectively. In another study, >50 % of the PDA detached from a PDA-coated PP film during submersion in acidic or alkaline conditions [63]. During the first 2 h, the detachment reached a threshold after which the PDA coating remained stable for the experiment duration of 12 h [63].

In the current study, the amount of remaining AgNP after the biofouling experiment was a fraction of the initial amount deposited on the spacers. In static batch experiments, Ronen et al. [19] observed a daily weight loss of AgNP from the spacer surface of 0.003–0.041 %. However, under hydrodynamic shear conditions, more leaching of AgNP and other nanoparticles from PDA-coated membrane surfaces was observed [57,64,65]. Liu et al. [57] reported a decline in the copper nanoparticle (CuNP) loading on the membrane surface of about 70 % during the first 2 days of operation. After 2 days the CuNP loading remained stable until the end of the experiment after 12 days of operation. The initial release was attributed to the leaching of weakly bound nanoparticles in the CuNP–PDA matrix under hydraulic sheer. We hypothesize that in our study, weakly bound AgNP was quickly released at the beginning of the experiment while the strongly bound AgNP remained on the surface. The largest amount of AgNP (~0.156 % *w*/w of the spacer) was released from the PDA–AgNP coating. Despite the leaching of AgNP, the CIP effectiveness of the PDA–AgNP-coated spacers remained constant through consecutive cycles, suggesting that sequestering a small amount of AgNP on a PDA coating can significantly improve the CIP effectiveness.

The lifetime of commercial membrane modules is several years, involving many CIP events [21]. Although the lifetimes of an uncoated and a coated PP feed spacer are equivalent, the benefits of the coating may diminish when AgNP and PDA are gradually released from the spacer surface over time. In the current study, the presence of PDA and AgNP on the modified feed spacers was still observed after 8 days of operation including two CIP events with 1 h recirculation of 0.1 % NaOH followed by 1 h recirculation of 0.2 % HCl. This observation suggests that the PDA coating adhered well to the spacer surface after cold plasma treatment, although minor deteriorations of the spacer coating cannot be observed in this way. Hence, the long-term mechanical stability under industrial operating conditions should be addressed in future work. Additionally, the possibility of reapplication through in-situ coating may be evaluated [66].

Finally, the release of toxic AgNP and silver ions are the main antimicrobial mechanisms of AgNP modified-coatings [67]. The release of AgNP enables improved CIP effectiveness, thereby reducing the CIP frequency, operational costs, and environmental impact. At the same time, the release of silver nanoparticles should be minimized to extend the spacer lifetime and to mitigate environmental and health risks from AgNP in the concentrate and permeate. Therefore, future studies should further explore this tradeoff to find a good balance between operational performance, durability, and environmental impact.

5. Conclusions

This study evaluated the biofouling development and CIP effectiveness of PP feed spacers modified with PDA, AgNP, and combined PDA–AgNP. Tests were performed in six membrane fouling simulators under operating conditions representing the industrial conditions of spiral-

wound membrane modules. The modification of the feed spacers did not delay the initial biofilm formation. However, the amount of remaining biofilm after CIP was significantly lower in the PDA- and combined PDA–AgNP-modified feed spacers than in the unmodified PP feed spacer. Owing to the improved CIP effectiveness, the biofouling rate and CIP frequency were greatly reduced in the modified spacers. Although the AgNP were partially leached between the start and end of the biofouling experiment, the PDA–AgNP-coated spacers retained their CIP effectiveness during consecutive operational cycles, suggesting that sequestering a small amount of AgNP on a PDA coating can significantly improve the CIP effectiveness. Our results revealed the importance of testing novel coatings over the full operational cycle. Coating the spacer with PDA and combined PDA–AgNP did not delay the biofilm formation but substantially improved the CIP effectiveness, thereby reducing the CIP frequency and operational costs.

CRediT authorship contribution statement

Kees Theo Huisman: Writing – original draft, Visualization, Validation, Methodology, Investigation, Formal analysis, Data curation, Conceptualization. **Mohamed H. Abdellah:** Writing – original draft, Methodology, Investigation, Formal analysis, Data curation, Conceptualization. **Damaris S. Alvarez Sosa:** Formal analysis, Data curation. **Filipa R. Fernandes Simoes:** Formal analysis, Data curation. **Bastiaan Blankert:** Writing – review & editing, Writing – original draft, Methodology, Investigation. **Johannes S. Vrouwenvelder:** Writing – review & editing, Supervision, Resources, Project administration, Methodology, Conceptualization. **Gyorgy Szekely:** Writing – review & editing, Supervision, Resources, Project administration, Methodology, Conceptualization.

Declaration of competing interest

The authors declare that they have no known competing financial interests or personal relationships that could have appeared to influence the work reported in this paper.

Data availability

Data will be made available on request.

Acknowledgment

The research reported in this publication was supported by funding from King Abdullah University of Science and Technology (KAUST) under BAS/1/1401-01-01 and IED OSR-2019-4455.

Appendix A. Supplementary data

Supplementary data to this article can be found online at https://doi.org/10.1016/j.desal.2024.117604.

References

[1] A.N. Bdour, M.R. Hamdi, Z. Tarawneh, Perspectives on sustainable wastewater treatment technologies and reuse options in the urban areas of the Mediterranean region, Desalination 237 (1) (2009) 162–174, https://doi.org/10.1016/j.desal.2007.12.030.

[2] M. Elimelech, W.A. Phillip, The future of seawater desalination: energy, Technology, and the Environment, Science 333 (6043) (2011) 712–717, https://doi.org/10.1126/science.1200488.

[3] G.A. Fimbres-Weihs, D.E. Wiley, Numerical study of mass transfer in three-dimensional spacer-filled narrow channels with steady flow, J. Membr. Sci. 306 (1) (2007) 228–243, https://doi.org/10.1016/j.memsci.2007.08.043.

[4] S.S. Bucs, N. Farhat, J.C. Kruithof, C. Picioreanu, M.C.M. van Loosdrecht, J. S. Vrouwenvelder, Review on strategies for biofouling mitigation in spiral wound membrane systems, Desalination 434 (2018) 189–197, https://doi.org/10.1016/j.desal.2018.01.023.

[5] H.-C. Flemming, Reverse osmosis membrane biofouling, Exp. Thermal Fluid Sci. 14 (4) (1997) 382–391, https://doi.org/10.1016/S0894-1777(96)00140-9.

[6] J.S. Vrouwenvelder, D.A. Graf von der Schulenburg, J.C. Kruithof, M.L. Johns, M.C. M. van Loosdrecht, Biofouling of spiral-wound nanofiltration and reverse osmosis membranes: a feed spacer problem, Water Res. 43 (3) (2009) 583–594, https://doi.org/10.1016/j.watres.2008.11.019.

[7] J. Yu, D. Chen, J.J. Wu, B. Wang, R.W. Field, Arch-type feed spacer with wide passage node design for spiral-wound membrane filtration with reduced energy cost, Desalination 540 (2022) 115980, https://doi.org/10.1016/j.desal.2022.115980.

[8] S.M. Ali, A. Qamar, S. Kerdi, S. Phuntsho, J.S. Vrouwenvelder, N. Ghaffour, H. K. Shon, Energy efficient 3D printed column type feed spacer for membrane filtration, Water Res. 164 (2019) 114961, https://doi.org/10.1016/j.watres.2019.114961.

[9] S. Park, Y.D. Jeong, J.H. Lee, J. Kim, K. Jeong, K.H. Cho, 3D printed honeycomb-shaped feed channel spacer for membrane fouling mitigation in nanofiltration, J. Membr. Sci. 620 (2021) 118665, https://doi.org/10.1016/j.memsci.2020.118665.

[10] N. Sreedhar, N. Thomas, N. Ghaffour, H.A. Arafat, The evolution of feed spacer role in membrane applications for desalination and water treatment: a critical review and future perspective, Desalination 554 (2023) 116505, https://doi.org/10.1016/j.desal.2023.116505.

[11] H.S. Abid, D.J. Johnson, R. Hashaikeh, N. Hilal, A review of efforts to reduce membrane fouling by control of feed spacer characteristics, Desalination 420 (2017) 384–402, https://doi.org/10.1016/j.desal.2017.07.019.

[12] M.A. Shannon, P.W. Bohn, M. Elimelech, J.G. Georgiadis, B.J. Mariñas, A. M. Mayes, Science and technology for water purification in the coming decades, Nature 452 (7185) (2008) 301–310, https://doi.org/10.1038/nature06599.

[13] W. Lin, Y. Zhang, D. Li, X.-m. Wang, X. Huang, Roles and performance enhancement of feed spacer in spiral wound membrane modules for water treatment: a 20-year review on research evolvement, Water Res. 198 (2021) 117146. doi:https://doi.org/10.1016/j.watres.2021.117146.

[14] P.A. Araújo, J.C. Kruithof, M.C.M. Van Loosdrecht, J.S. Vrouwenvelder, The potential of standard and modified feed spacers for biofouling control, J. Membr. Sci. 403-404 (2012) 58–70, https://doi.org/10.1016/j.memsci.2012.02.015.

[15] C. Liu, Z. Wang, Q. He, J. Jackson, A.F. Faria, W. Zhang, D. Song, J. Ma, Z. Sun, Facile preparation of anti-biofouling reverse osmosis membrane embedded with polydopamine-nano copper functionality: performance and mechanism, J. Membr. Sci. 658 (2022) 120721, https://doi.org/10.1016/j.memsci.2022.120721.

[16] F. Li, J. Meng, J. Ye, B. Yang, Q. Tian, C. Deng, Surface modification of PES ultrafiltration membrane by polydopamine coating and poly(ethylene glycol) grafting: morphology, stability, and anti-fouling, Desalination 344 (2014) 422–430, https://doi.org/10.1016/j.desal.2014.04.011.

[17] D.J. Miller, P.A. Araújo, P.B. Correia, M.M. Ramsey, J.C. Kruithof, M.C.M. van Loosdrecht, B.D. Freeman, D.R. Paul, M. Whiteley, J.S. Vrouwenvelder, Short-term adhesion and long-term biofouling testing of polydopamine and poly(ethylene glycol) surface modifications of membranes and feed spacers for biofouling control, Water Res. 46 (12) (2012) 3737–3753, https://doi.org/10.1016/j.watres.2012.03.058.

[18] H.-L. Yang, J.C.-T. Lin, C. Huang, Application of nanosilver surface modification to RO membrane and spacer for mitigating biofouling in seawater desalination, Water Res. 43 (15) (2009) 3777–3786, https://doi.org/10.1016/j.watres.2009.06.002.

[19] A. Ronen, S. Lerman, G.Z. Ramon, C.G. Dosoretz, Experimental characterization and numerical simulation of the anti-biofuling activity of nanosilver-modified feed spacers in membrane filtration, J. Membr. Sci. 475 (2015) 320–329, https://doi.org/10.1016/j.memsci.2014.10.042.

[20] P.A. Araújo, D.J. Miller, P.B. Correia, M.C.M. van Loosdrecht, J.C. Kruithof, B. D. Freeman, D.R. Paul, J.S. Vrouwenvelder, Impact of feed spacer and membrane modification by hydrophilic, bactericidal and biocidal coating on biofouling control, Desalination 295 (2012) 1–10, https://doi.org/10.1016/j.desal.2012.02.026.

[21] Dow Water & Process Solutions, FILMTEC™ Reverse Osmosis Membranes Technical Manual.

[22] W. Lawler, J. Alvarez-Gaitan, G. Leslie, P. Le-Clech, Comparative life cycle assessment of end-of-life options for reverse osmosis membranes, Desalination 357 (2015) 45–54, https://doi.org/10.1016/j.desal.2014.10.013.

[23] E. Arkhangelsky, D. Kuzmenko, N.V. Gitis, M. Vinogradov, S. Kuiry, V. Gitis, Hypochlorite cleaning causes degradation of polymer membranes, Tribol. Lett. 28 (2) (2007) 109–116, https://doi.org/10.1007/s11249-007-9253-6.

[24] Q. Huang, J. Chen, M. Liu, H. Huang, X. Zhang, Y. Wei, Polydopamine-based functional materials and their applications in energy, environmental, and catalytic fields: state-of-the-art review, Chem. Eng. J. 387 (2020) 124019, https://doi.org/10.1016/j.cej.2020.124019.

[25] T.M. Aminabhavi, S.P. Dharupaneedi, U.A. More, 1 - the role of nanotechnology and chitosan-based biomaterials for tissue engineering and therapeutic delivery, in: J.A. Jennings, J.D. Bumgardner (Eds.), Chitosan Based Biomaterials Volume 2, Woodhead Publishing, 2017, pp. 1–29, https://doi.org/10.1016/B978-0-08-100228-5.00001-8.

[26] S.-G. Park, P.P. Rajesh, M.-H. Hwang, K.H. Chu, S. Cho, K.-J. Chae, Long-term effects of anti-biofouling proton exchange membrane using silver nanoparticles and polydopamine on the performance of microbial electrolysis cells, Int. J. Hydrog. Energy 46 (20) (2021) 11345–11356, https://doi.org/10.1016/j.ijhydene.2020.04.059.

[27] D. Zhao, J.F. Kim, G. Ignacz, P. Pogany, Y.M. Lee, G. Szekely, Bio-inspired robust membranes nanoengineered from interpenetrating polymer networks of

polybenzimidazole/polydopamine, ACS Nano 13 (1) (2019) 125–133, https://doi.org/10.1021/acsnano.8b04123.
[28] I. Singh, G. Dhawan, S. Gupta, P. Kumar, Recent advances in a polydopamine-mediated antimicrobial adhesion system, Front. Microbiol. 11 (2021), https://doi.org/10.3389/fmicb.2020.607099.
[29] D.G. Barrett, T.S. Sileika, P.B. Messersmith, Molecular diversity in phenolic and polyphenolic precursors of tannin-inspired nanocoatings, Chem. Commun. 50 (55) (2014) 7265–7268, https://doi.org/10.1039/C4CC02961E.
[30] C. Zhang, J. Jin, J. Zhao, W. Jiang, J. Yin, Functionalized polypropylene non-woven fabric membrane with bovine serum albumin and its hemocompatibility enhancement, Colloids Surf. B: Biointerfaces 102 (2013) 45–52, https://doi.org/10.1016/j.colsurfb.2012.08.007.
[31] L. Zhu, Y. Lu, Y. Wang, L. Zhang, W. Wang, Preparation and characterization of dopamine-decorated hydrophilic carbon black, Appl. Surf. Sci. 258 (14) (2012) 5387–5393, https://doi.org/10.1016/j.apsusc.2012.02.016.
[32] L. Liu, R. Cai, Y. Wang, G. Tao, L. Ai, P. Wang, M. Yang, H. Zuo, P. Zhao, H. He, Polydopamine-assisted silver nanoparticle self-assembly on sericin/agar film for potential wound dressing application, Int. J. Mol. Sci. 19 (10) (2018) 2875.
[33] K.T. Huisman, N. Franco-Clavijo, J.S. Vrouwenvelder, B. Blankert, Improved quantitative evaluation of the fouling potential in spacer-filled membrane filtration channels through a biofouling index based on the relative pressure drop, J. Membr. Sci. 671 (2023) 121400, https://doi.org/10.1016/j.memsci.2023.121400.
[34] J.S. Vrouwenvelder, M.C.M. van Loosdrecht, J.C. Kruithof, Early warning of biofouling in spiral wound nanofiltration and reverse osmosis membranes, Desalination 265 (1) (2011) 206–212, https://doi.org/10.1016/j.desal.2010.07.053.
[35] J.S. Vrouwenvelder, J.A.M. van Paassen, L.P. Wessels, A.F. van Dam, S.M. Bakker, The membrane fouling simulator: a practical tool for fouling prediction and control, J. Membr. Sci. 281 (1) (2006) 316–324, https://doi.org/10.1016/j.memsci.2006.03.046.
[36] J.S. Vrouwenvelder, C. Hinrichs, W.G.J. Van der Meer, M.C.M. Van Loosdrecht, J. C. Kruithof, Pressure drop increase by biofilm accumulation in spiral wound RO and NF membrane systems: role of substrate concentration, flow velocity, substrate load and flow direction, Biofouling 25 (6) (2009) 543–555, https://doi.org/10.1080/08927010902972225.
[37] S.S. Bucs, R. Valladares Linares, J.O. Marston, A.I. Radu, J.S. Vrouwenvelder, C. Picioreanu, Experimental and numerical characterization of the water flow in spacer-filled channels of spiral-wound membranes, Water Res. 87 (2015) 299–310, https://doi.org/10.1016/j.watres.2015.09.036.
[38] E.M.V. Hoek, J. Allred, T. Knoell, B.-H. Jeong, Modeling the effects of fouling on full-scale reverse osmosis processes, J. Membr. Sci. 314 (1) (2008) 33–49, https://doi.org/10.1016/j.memsci.2008.01.025.
[39] J.S. Vrouwenvelder, J.A.M. van Paassen, J.C. Kruithof, M.C.M. van Loosdrecht, Sensitive pressure drop measurements of individual lead membrane elements for accurate early biofouling detection, J. Membr. Sci. 338 (1) (2009) 92–99, https://doi.org/10.1016/j.memsci.2009.04.016.
[40] K.T. Huisman, L. Fortunato, J.S. Vrouwenvelder, B. Blankert, A clear view of biofouling in spacer filled membrane filtration channels: integrating OCT and CT for improved visualization and localization, J. Membr. Sci. 697 (2024) 122573, https://doi.org/10.1016/j.memsci.2024.122573.
[41] K.T. Huisman, B. Blankert, H. Horn, M. Wagner, J.S. Vrouwenvelder, S. Bucs, L. Fortunato, Noninvasive monitoring of fouling in membrane processes by optical coherence tomography: a review, J. Membr. Sci. 692 (2024) 122291, https://doi.org/10.1016/j.memsci.2023.122291.
[42] C. Li, J. Zhang, J. Han, B. Yao, A numerical solution to the effects of surface roughness on water–coal contact angle, Sci. Rep. 11 (1) (2021) 459, https://doi.org/10.1038/s41598-020-80729-9.
[43] Y. Coffinier, G. Piret, M.R. Das, R. Boukherroub, Effect of surface roughness and chemical composition on the wetting properties of silicon-based substrates, C. R. Chim. 16 (1) (2013) 65–72, https://doi.org/10.1016/j.crci.2012.08.011.
[44] L. Fortunato, T. Leiknes, In-situ biofouling assessment in spacer filled channels using optical coherence tomography (OCT): 3D biofilm thickness mapping, Bioresour. Technol. 229 (2017) 231–235, https://doi.org/10.1016/j.biortech.2017.01.021.
[45] F.R.F. Simoes, N.M. Batra, B.H. Warsama, C.G. Canlas, S. Patole, T.F. Yapici, P.M.F. J. Costa, Elemental quantification and residues characterization of wet digested certified and commercial carbon materials, Anal. Chem. 88 (23) (2016) 11783–11790, https://doi.org/10.1021/acs.analchem.6b03407.
[46] R.M. Donlan, Biofilms: microbial life on surfaces, Emerg. Infect. Dis. 8 (9) (2002) 881–890, https://doi.org/10.3201/eid0809.020063.
[47] A. Gjaltema, N. Van Der Marel, M.C.M. Van Loosdrecht, J.J. Heijnen, Adhesion and biofilm development on suspended carriers in airlift reactors: hydrodynamic conditions versus surface characteristics, Biotechnol. Bioeng. 55 (6) (1997) 880–889, https://doi.org/10.1002/(SICI)1097-0290(19970920)55:6<880::AID-BIT6>3.0.CO;2-C.
[48] Y. Baek, J. Yu, S.-H. Kim, S. Lee, J. Yoon, Effect of surface properties of reverse osmosis membranes on biofouling occurrence under filtration conditions, J. Membr. Sci. 382 (1) (2011) 91–99, https://doi.org/10.1016/j.memsci.2011.07.049.
[49] A. Subramani, E.M.V. Hoek, Direct observation of initial microbial deposition onto reverse osmosis and nanofiltration membranes, J. Membr. Sci. 319 (1) (2008) 111–125, https://doi.org/10.1016/j.memsci.2008.03.025.
[50] W.S. Ang, S. Lee, M. Elimelech, Chemical and physical aspects of cleaning of organic-fouled reverse osmosis membranes, J. Membr. Sci. 272 (1) (2006) 198–210, https://doi.org/10.1016/j.memsci.2005.07.035.
[51] W.S. Ang, N.Y. Yip, A. Tiraferri, M. Elimelech, Chemical cleaning of RO membranes fouled by wastewater effluent: achieving higher efficiency with dual-step cleaning, J. Membr. Sci. 382 (1) (2011) 100–106, https://doi.org/10.1016/j.memsci.2011.07.047.
[52] P. Desmond, K.T. Huisman, H. Sanawar, N.M. Farhat, J. Traber, E.O. Fridjonsson, M.L. Johns, H.-C. Flemming, C. Picioreanu, J.S. Vrouwenvelder, Controlling the hydraulic resistance of membrane biofilms by engineering biofilm physical structure, Water Res. 210 (2022) 118031, https://doi.org/10.1016/j.watres.2021.118031.
[53] T. Seviour, N. Derlon, M.S. Dueholm, H.-C. Flemming, E. Girbal-Neuhauser, H. Horn, S. Kjelleberg, M.C.M. van Loosdrecht, T. Lotti, M.F. Malpei, R. Nerenberg, T.R. Neu, E. Paul, H. Yu, Y. Lin, Extracellular polymeric substances of biofilms: suffering from an identity crisis, Water Res. 151 (2019) 1–7, https://doi.org/10.1016/j.watres.2018.11.020.
[54] W. Lee, C.H. Ahn, S. Hong, S. Kim, S. Lee, Y. Baek, J. Yoon, Evaluation of surface properties of reverse osmosis membranes on the initial biofouling stages under no filtration condition, J. Membr. Sci. 351 (1) (2010) 112–122, https://doi.org/10.1016/j.memsci.2010.01.035.
[55] N.K. Khanzada, S. Rehman, S.-Y. Leu, A.K. An, Evaluation of anti-bacterial adhesion performance of polydopamine cross-linked graphene oxide RO membrane via in situ optical coherence tomography, Desalination 479 (2020) 114339, https://doi.org/10.1016/j.desal.2020.114339.
[56] B.P. Tripathi, P. Das, F. Simon, M. Stamm, Ultralow fouling membranes by surface modification with functional polydopamine, Eur. Polym. J. 99 (2018) 80–89, https://doi.org/10.1016/j.eurpolymj.2017.12.006.
[57] C. Liu, Q. He, D. Song, J. Jackson, A.F. Faria, X. Jiang, X. Li, J. Ma, Z. Sun, Electroless deposition of copper nanoparticles integrates polydopamine coating on reverse osmosis membranes for efficient biofouling mitigation, Water Res. 217 (2022) 118375, https://doi.org/10.1016/j.watres.2022.118375.
[58] A. Al Ashhab, A. Sweity, B. Bayramoglu, M. Herzberg, O. Gillor, Biofouling of reverse osmosis membranes: effects of cleaning on biofilm microbial communities, membrane performance, and adherence of extracellular polymeric substances, Biofouling 33 (5) (2017) 397–409, https://doi.org/10.1080/08927014.2017.1318382.
[59] M.C. Hacıfazlıoğlu, İ. Parlar, T.Ö. Pek, N. Kabay, Evaluation of chemical cleaning to control fouling on nanofiltration and reverse osmosis membranes after desalination of MBR effluent, Desalination 466 (2019) 44–51, https://doi.org/10.1016/j.desal.2019.05.003.
[60] H. Sanawar, L.H. Kim, N.M. Farhat, M.C.M. van Loosdrecht, J.S. Vrouwenvelder, Periodic chemical cleaning with urea: disintegration of biofilms and reduction of key biofilm-forming bacteria from reverse osmosis membranes, Water Research X 13 (2021) 100117, https://doi.org/10.1016/j.wroa.2021.100117.
[61] Y. Wibisono, W. Yandi, M. Golabi, R. Nugraha, Emile R. Cornelissen, A.J. B. Kemperman, T. Ederth, K. Nijmeijer, Hydrogel-coated feed spacers in two-phase flow cleaning in spiral wound membrane elements: a novel platform for eco-friendly biofouling mitigation, Water Res. 71 (2015) 171–186, https://doi.org/10.1016/j.watres.2014.12.030.
[62] W. Yang, C. Liu, Y. Chen, Stability of polydopamine coatings on gold substrates inspected by surface plasmon resonance imaging, Langmuir 34 (12) (2018) 3565–3571, https://doi.org/10.1021/acs.langmuir.7b03143.
[63] H. Wei, J. Ren, B. Han, L. Xu, L. Han, L. Jia, Stability of polydopamine and poly (DOPA) melanin-like films on the surface of polymer membranes under strongly acidic and alkaline conditions, Colloids Surf. B: Biointerfaces 110 (2013) 22–28, https://doi.org/10.1016/j.colsurfb.2013.04.008.
[64] K.P. Wai, C.H. Koo, Y.L. Pang, W.C. Chong, W.J. Lau, In situ immobilization of silver on polydopamine-coated composite membrane for enhanced antibacterial properties, Journal of Water Process Engineering 33 (2020) 100989, https://doi.org/10.1016/j.jwpe.2019.100989.
[65] M.S.S.A. Saraswathi, D. Rana, S. Alwarappan, S. Gowrishankar, P. Vijayakumar, A. Nagendran, Polydopamine layered poly (ether imide) ultrafiltration membranes tailored with silver nanoparticles designed for better permeability, selectivity and antifouling, J. Ind. Eng. Chem. 76 (2019) 141–149, https://doi.org/10.1016/j.jiec.2019.03.014.
[66] M.F. Nava-Ocampo, S.S. Bucs, A.S.F. Farinha, M. Son, B.E. Logan, J. S. Vrouwenvelder, Sacrificial coating development for biofouling control in membrane systems, Desalination 496 (2020) 114650, https://doi.org/10.1016/j.desal.2020.114650.
[67] N. Durán, M. Durán, M.B. de Jesus, A.B. Seabra, W.J. Fávaro, G. Nakazato, Silver nanoparticles: a new view on mechanistic aspects on antimicrobial activity, Nanomedicine 12 (3) (2016) 789–799, https://doi.org/10.1016/j.nano.2015.11.016.